Monthly Notices
of the
ROYAL ASTRONOMICAL SOCIETY

MNRAS **468,** 4441–4449 (2017)
Advance Access publication 2017 March 17

doi:10.1093/mnras/stx663

Long-term evolution of initially unvirialized, clumpy, mass-segregated star clusters in tidal fields

L. J. Rossi,[1]★ J. R. Hurley[1] and K. Bekki[2]

[1]*Centre for Astrophysics and Supercomputing, Swinburne University of Technology, Hawthorn, VIC 3122, Australia*
[2]*ICRAR, M468, The University of Western Australia, 35 Stirling Hwy, Crawley, WA 6009, Australia*

Accepted 2017 March 13. Received 2017 March 3; in original form 2017 February 1

ABSTRACT

Star clusters can form in highly substructured configurations, possibly unvirialized and possibly with a primordial degree of mass segregation. None the less, a common assumption of many *N*-body simulations of star clusters is that the clusters are initially spherical, homogeneous and in virial equilibrium. The impact of the choice of the initial conditions on the long-term evolution of the clusters is unclear, considering also that the tidal field plays an important role in setting the mass-loss rate and size of dynamically evolved objects. We present a series direct *N*-body simulations of star clusters spanning a range of initial degree of clumpiness, virial state and mass segregation and following different trajectories in a realistic galactic tidal field. The results suggest that, even if the choice of the initial conditions has a non-negligible impact, the long-term evolution of a star cluster seems to be dominated by the tidal forces experienced along its trajectory in the host galaxy.

Key words: gravitation – methods: numerical – galaxies: star clusters: general – galaxies: structure.

1 INTRODUCTION

In recent years, considerable effort has been devoted to the development of self-consistent methods to investigate the history of the formation and evolution of star clusters in galaxies. From a computational perspective, in the ideal scenario, the formation sites of star clusters and their subsequent tidal history in the gravitational field of the host galaxy would be directly inferred from hydrodynamical and collisionless *N*-body simulations of galaxies, while their internal evolution would be followed by direct collisional *N*-body or Monte Carlo simulations. Because of computational challenges, much of the work to date has been devoted either to the study of the formation mechanisms and the initial global properties of star cluster populations in galaxies (e.g. Beasley et al. 2002; Bekki et al. 2002; Li, Mac Low & Klessen 2004; Kravtsov & Gnedin 2005; Bournaud, Duc & Emsellem 2008; Boley et al. 2009; Renaud, Bournaud & Duc 2015; Li et al. 2017) or on their subsequent dynamical evolution in galactic tidal fields (e.g. Baumgardt & Makino 2003; Renaud & Gieles 2013; Rieder et al. 2013; Rossi, Bekki & Hurley 2016). As a step forwards towards more self-consistent numerical modelling in a recent study, Renaud, Agertz & Gieles (2017) identified the formation sites and initial properties of star clusters in a Milky Way-like galaxy in a cosmological simulation and followed the subsequent environmental evolution through cosmic times in the form of tidal tensors. However, one problem with this approach is that the time-scale and spatial resolution required in numerical simulations of galaxies and star clusters differ by several orders of magnitude and the resolution required to self-consistently simulate the details of the star-cluster-forming regions in galaxy-scale simulations is still out of reach. Furthermore, even a dedicated numerical simulation of a star cluster formation from a molecular cloud with individual star formation resolved is computationally too expensive to model the birth of the most massive cluster, although progress can be made by reducing the resolution of the simulations (e.g. Dale, Ercolano & Bonnell 2012).

Star clusters form in highly substructured configurations. Highly turbulent molecular clouds fragment in clumps and filaments within which star formation occurs, as seen both in observations (e.g. Gutermuth et al. 2009; Schneider et al. 2012; Rathborne et al. 2015) and in numerical simulations of star cluster formation (e.g. Bate, Bonnell & Bromm 2003; Bonnell, Bate & Vine 2003; Bonnell, Clark & Bate 2008; Fujii 2015). Both theory and observation favour a scenario in which the majority of a star-forming cluster is characterized by subvirial velocities of the stars (Girichidis et al. 2012), and virialization is expected to occur on a very short time-scale (Lada, Margulis & Dearborn 1984). The exact value of the primordial virial ratio could have an important effect on the early dynamical evolution of a cluster (Allison et al. 2010; Caputo, de Vries & Portegies Zwart 2014). Furthermore, there is evidence that clusters should likely form unsegregated (Girichidis et al. 2012) or with a certain small degree of primordial mass segregation (Bonnell &

★ E-mail: lucarossi@swin.edu.au

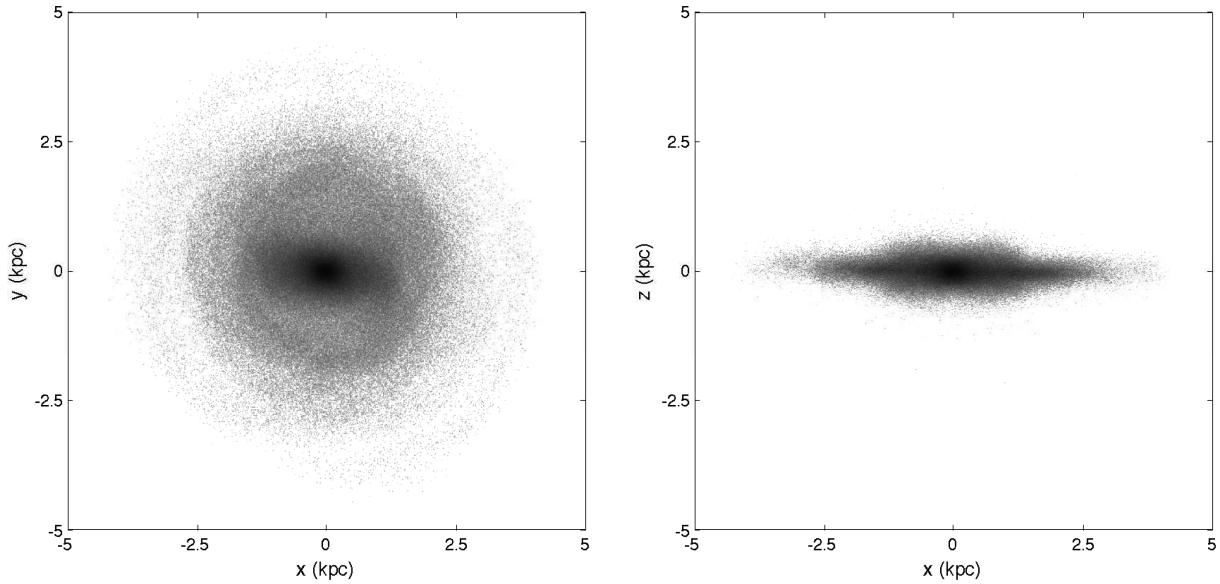

Figure 1. Face-on (left-hand panel) and edge-on (right-hand panel) snapshot of the evolution of the adopted galaxy model.

Davies 1998). Moeckel & Bonnell (2009) explored the evolution of very young clusters from a primordially segregated state with *N*-body simulations, concluding that, in general, initially mass-segregated clusters evolve towards configurations that are inconsistent with the observations of young clusters. However, despite the complexity of the physical processes involved in the early evolutionary stages, a very common assumption in works presenting the results of *N*-body simulations of star clusters is that the clusters are initially in a spherical, virialized configuration. The suspicion that such an assumption could miss some important pieces of information has been raised by the results of Goodwin & Whitworth (2004), amongst others, in which the authors investigated the early dynamical evolution of unvirialized fractal star clusters and found that the initial velocity dispersion of the stars and the virial state of the clusters have a strong impact on the initial phases of the clusters' life. Following these lines, Parker et al. (2014) showed that initial fractal degree and virial state of a star-forming region can impact the evolution of the degree of substructure, dynamical mass segregation and local density around stars as a function of the stellar mass.

After the early stages dominated by stellar evolution effects, the subsequent dynamical history of a cluster is strongly influenced by the galactic tidal field (and by relaxation). For example, the mass-loss rate, dissolution times and maximum size of the clusters can vary dramatically depending on the galactic orbit and the properties of the host galaxy. Whether the initial conditions of clusters could have an impact on the long-term evolution, following the concern of Goodwin & Whitworth (2004), or whether the tidal field still represents the dominant factor has not been quantitatively studied yet, and represents the major focus of the present analysis. In other words, our main goal is to check if the 'standard' assumption of initially spherical, homogeneous, virialized clusters is justifiable when studying star cluster dynamics in tidal fields or if more sophisticated modelling of the initial conditions is required.

In order to address such a question, we designed a numerical experiment in which we followed the long-term evolution of star clusters with different initial properties (clumpiness, virial ratios, mass segregation) and subject to different tidal forces. We then compared the evolved properties of the star clusters to examine the dependence on their initial conditions and galactic orbit. In Section 2, we present the numerical methods and procedures adopted to generate and then follow the evolution of the star clusters. The results of the *N*-body simulations are included in Section 3. Finally, in Section 4, we include a summary of our work and present our conclusions.

2 METHODS

2.1 Tidal field

The simulated clusters evolve within an *N*-body galaxy representative of the Large Magellanic Cloud (LMC), corresponding to the GAL6 model in Rossi et al. (2016). In this model, the stellar disc has an initial radius of 3 kpc and a mass of 9×10^8 $M_\odot$, while the dark matter halo has a radius of 41.7 kpc and a mass of 3×10^{10} $M_\odot$. We refer to the original paper for a more comprehensive description of the galaxy simulation. Fig. 1 shows a snapshot from the galaxy *N*-body simulation. The choice of the LMC model rather than, for example, a Milky Way model was based on the evidence that the LMC hosts massive clusters spanning a broad range of ages, providing a more global view of cluster populations (Portegies Zwart, McMillan & Gieles 2010). In order to evaluate the effect of different tidal fields, we chose two distinct orbits in the galaxy model. The inner orbit has perigalacticon and apogalacticon of $R_\mathrm{p} \sim 0.8$ kpc and $R_\mathrm{a} \sim 1.9$ kpc, respectively, corresponding to an eccentricity $e \sim 0.4$. The maximum excursion from the galactic plane is $z_\mathrm{max} \sim 0.8$ kpc. The outer orbit is confined between $R_\mathrm{p} \sim 0.9$ kpc and $R_\mathrm{a} \sim 6.2$ kpc, corresponding to $e \sim 0.7$. This outer trajectory has a maximum excursion from the galactic plane of $z_\mathrm{max} \sim 3$ kpc (see Fig. 2 for a visualization of the different trajectories on the galactic plane and on the meridional plane). The tidal histories of the first Gyr of evolution of a representative cluster following the selected trajectories are shown in the right-hand panels of Fig. 2, in terms of the magnitude of the acceleration as a function of time.

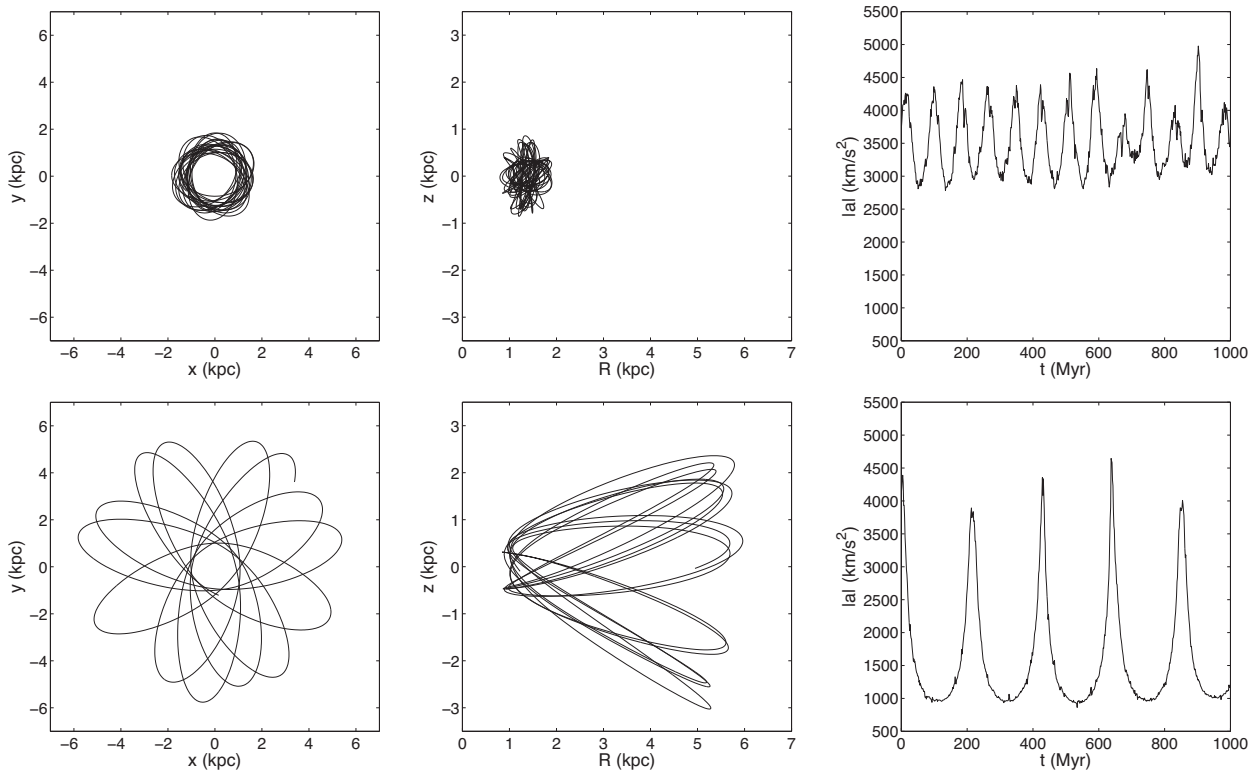

Figure 2. Left-hand panels: projection of the selected cluster trajectories on the galactic plane for the inner (top panel) and outer (bottom panel) orbits. Middle panels: projection of the selected cluster trajectories on the meridional plane for the inner (top panel) and outer (bottom panel) orbits. Right-hand panels: evolution of the magnitude of the gravitational field evaluated at the centre of mass of the cluster for the inner (top panel) and outer (bottom panel) orbits.

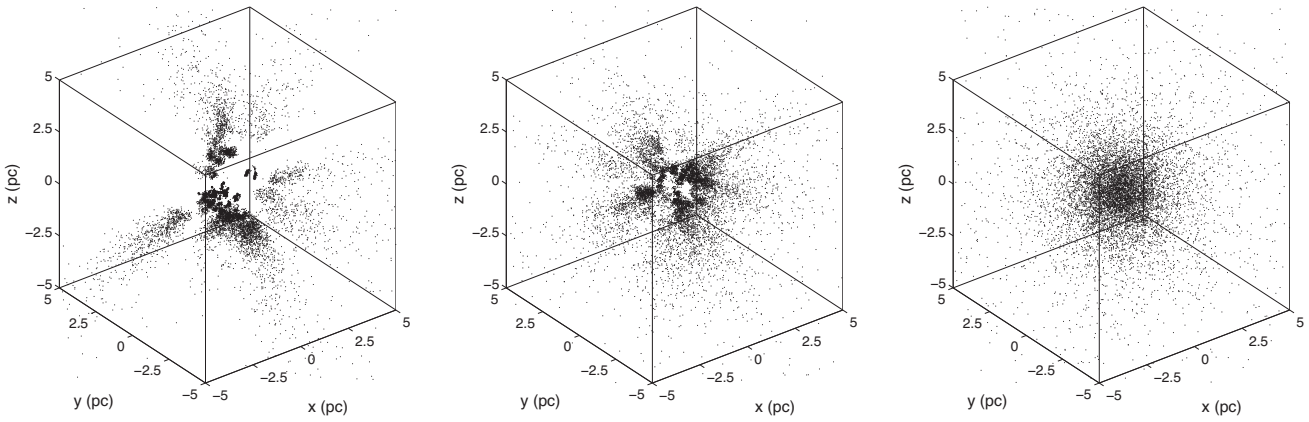

Figure 3. Initial configuration of stars for three different realizations of a cluster composed of 10k stars with fractal dimension $D = 1.6$ (left-hand panel), $D = 2.0$ (middle panel) and $D = 3.0$ (right-hand panel).

2.2 Initial conditions of the star clusters

As mentioned above, one of the common assumptions in many *N*-body simulations of star clusters is that the cluster members are distributed in a spherical configuration (typically a Plummer's sphere or a King model). In order to overcome this basic assumption, we generated initially clumpy, i.e. fractal, star clusters with the MCLUSTER code (Küpper et al. 2011). In essence, the fractal clusters follow a Plummer density profile (Plummer 1911) and the velocity of each star in the different fractal configurations is scaled to the expected velocity of a star at the given radius within such profile. We refer to Küpper et al. (2011) and to Goodwin & Whitworth (2004) for a detailed description of the procedure followed in the code to generate the fractal structures. The degree of fractality of a three-dimensional distribution of points can be quantified by a parameter *D*, called 'fractal dimension'. In this work, we considered three distinct realizations of fractal star clusters characterized by fractal dimensions $D = 1.6$, 2.0 and 3.0, corresponding to 6/8 fractal, 4/8 fractal and spherical clusters, respectively. Fig. 3 shows the three-dimensional structure of these realizations.

We also considered clusters in different initial virial states. The overall dynamical state of a self-gravitating system can be

Table 1. Combination of initial conditions of star cluster simulations considered in this work. $\alpha_{\rm vir}$, D and S are the primordial virial ratio, fractal dimension and mass segregation, respectively. For each of the two selected orbits (see Fig. 2), we generated three different realizations of each combination of different initial conditions for a total of 66 simulations.

	$\alpha_{\rm vir} = 0.2$	$\alpha_{\rm vir} = 0.5$	$\alpha_{\rm vir} = 0.8$
$D = 1.6$	$S = 0.0$	$S = 0.0$	$S = 0.0$
$D = 2.0$	$S = 0.0$	$S = 0.0$	$S = 0.0$
$D = 3.0$	$S = 0.0$	$S = 0.0$ $S = 0.5$ $S = 1.0$	$S = 0.0$

characterized by its virial ratio $\alpha_{\rm vir} = T/E$, where T is the total kinetic energy and E is the total gravitational potential energy. According to the fundamental result of the virial theorem, the system is in equilibrium when $\alpha_{\rm vir} = 0.5$. Subvirial clusters ($\alpha_{\rm vir} < 0.5$) are in a collapsing phase, while supervirial cluster ($\alpha_{\rm vir} > 0.5$) are in an expanding phase. In order to consider these different scenarios, we chose three different virial ratios for our simulated clusters, namely $\alpha_{\rm vir} = 0.2$. 0.5 and 0.8.

The effect of initial mass segregation has been taken into account as well. We quantified the degree of mass segregation with the parameter S, as defined within MCLUSTER (Küpper et al. 2011). The code generates different degrees of mass segregation as follows. First, the masses of the N stars are ordered in a decreasing order from highest to lowest in a mass array. Likewise, the stars are ordered in a position array according to their distance from the origin of the coordinates, where the first star is the closest. The masses are then written to a new array, beginning from the highest mass, where the ith massive star is placed in the array element with index j, generated by the equation

$$j = (N - i)(1 - X^{1-S}), \quad (1)$$

where X is a random number between 0 and 1 and S is the mass segregation parameter. The masses are then assigned to each star by matching the new mass array with the position array. According to this definition, $S = 0.0$ implies a random distribution for the masses, $S = 1.0$ implies a perfectly ordered array and values of S between 0 and 1 produce intermediate degrees of mass segregation. In the present analysis, we only considered the case of initially spherical and virialized mass-segregated clusters with degrees of mass segregation of $S = 0.0$, 0.5 and 1.0.

We then generated homogeneous ($S = 0$) clusters spanning each combination of the selected initial values of D and $\alpha_{\rm vir}$ (nine different combinations). On top of that, we generated spherical, virialized clusters with varying degree of primordial mass segregation S, for a total of 11 different initial conditions. The number of combinations doubles when considering the two different orbits, leading to 22 distinct initial conditions. Furthermore, for each initial combination of D, $\alpha_{\rm vir}$, S and orbit, we generated three different realizations of the clusters with different seed number to take into account stochastic effects for a total of 66 direct N-body simulations (see Table 1).

The N-body simulations of the star clusters were performed with NBODY6 (Aarseth 2003). In this study, we adopted the modified version of the code described in Rossi et al. (2016) to take into account the tidal field generated by the N-body galaxy. Our simulated star clusters are initially composed of 10 k stars with a selected 5 per cent fraction of primordial binaries. Single stellar evolution (Hurley, Pols & Tout 2000) and binary stellar evolution (Hurley, Tout & Pols 2002) are included. A Kroupa mass function (Kroupa 2001) is assumed for the initial distribution of the stellar masses, and we selected a metallicity [Fe/H] $= -1.4$ for all the models. All the realizations of the clusters are characterized by an initial half-mass radius $r_{\rm hm} = 2$ pc, unless otherwise specified.

As a Plummer sphere is in principle infinitely extended, we impose a truncation of the stellar distribution. The cut-off radius is set to be equal to the initial theoretical tidal radius of the cluster, which in turn depends on its initial mass and on the intensity of the external gravitational field (see Rossi et al. 2016). For example, the initial tidal radius of the clusters following the selected inner orbit and starting with $N = 10^4$ stars is about 20 pc. However, we also note that for the Plummer model the vast majority of the stars are confined within a distance of about twice the initial half-mass radius.

In the simulations, we assume a star to have escaped the cluster if it reaches a distance from the centre of mass of the cluster equal to twice the size of the tidal radius with positive total energy. Once a star escapes the system, it is automatically removed from the N-body simulation.

3 RESULTS: LONG-TERM EFFECT OF DIFFERENT INITIAL CONDITIONS

In order to compare how different initial conditions influence the subsequent evolution of some of the main properties of the clusters, we selected an appropriate reference time at which such properties are evaluated. For this analysis, we chose $t_{\rm check} = 500$ Myr, at which point the clusters with 10k stars on the selected orbits have generally lost at least 50 per cent of their mass but still retained a significant fraction of their initial mass (greater than about 20 per cent). This ensures that clusters are evolved, but small-N fluctuations at late stages are avoided.

We analysed how different initial conditions affect three of the main observable properties of star clusters, namely the mass, the size (quantified in terms of the half-mass radius) and the velocity dispersion. We adopted the average value of these parameters, defined as the mean of the three different number-seed realizations of the clusters for each (D, $\alpha_{\rm vir}$, S, orbit) combination and assigned an error defined as the standard deviation from the average value.

3.1 Impact of the initial fractal dimension on the long-term evolution

We first focus on the degree of fractality. As shown in the left-hand panel of Fig. 4, the results of the N-body simulations suggest that the initial fractal dimension D mildly impacts the evolution of the selected cluster properties. When considering the average values, we found an increasing trend of retained mass for increasing values of the fractal dimension. Clusters with the smaller initial D (i.e. more clumpy clusters) at $t_{\rm check}$ have lost typically 5–10 per cent more of the initial mass compared with initial spherical configurations. An example is shown in the left-hand panel of Fig. 5, where we plotted the evolution of the mass for three realizations of clusters on the outer orbit with initial $\alpha_{\rm vir} = 0.8$ and different initial fractal dimensions. The increasing initial fractal dimension results in only slightly decreasing mass-loss rates. It is plausible to expect that mass-loss may be enhanced in clumpy clusters when we consider the impact of the presence of substructure on the relaxation time of a cluster. We recall that the relaxation time is proportional to the number of stars in the cluster and to the crossing time. The relaxation time of the various substructures in a clumpy cluster is expected to be smaller than the relaxation time of a spherical cluster, which mirrors higher mass-loss rates. For example, if the

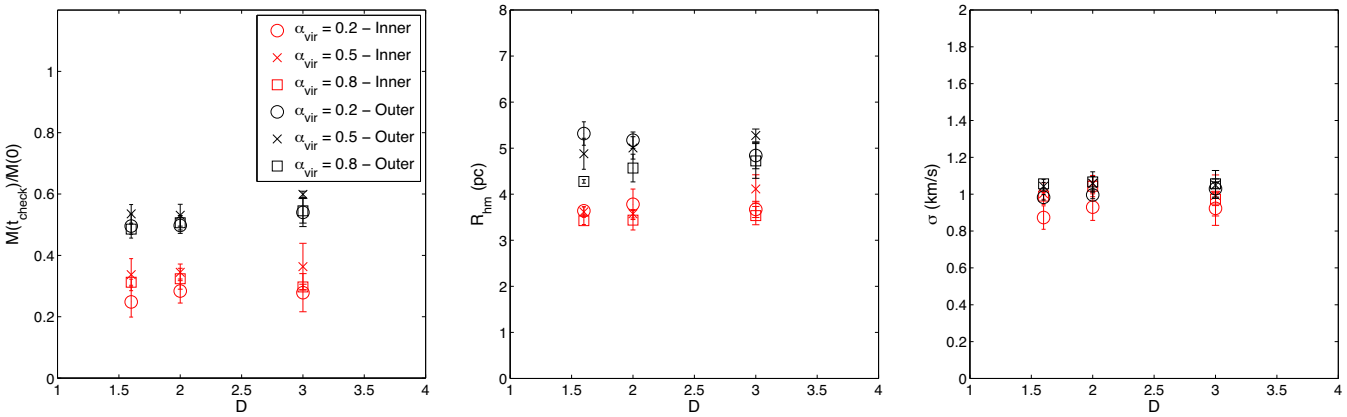

Figure 4. Left-hand panel: fraction of the initial mass retained by the star clusters at $t_{\rm check}$ as a function of the initial fractal degree D for clusters with different initial virial ratios. The open circles, crosses and open squares show the average value for clusters with $\alpha_{\rm vir} = 0.2$, 0.5 and 0.8, respectively. The red and black symbols show the results for the inner orbit and the outer orbit, respectively. Middle panel: half-mass radius at $t_{\rm check}$ as a function of the initial fractal degree D for clusters with different initial virial ratios. Symbols as in the left-hand panel. Right-hand panel: velocity dispersion of the cluster members at $t_{\rm check}$ as a function of the initial fractal degree D for clusters with different initial virial ratios. Symbols as in the left-hand panel.

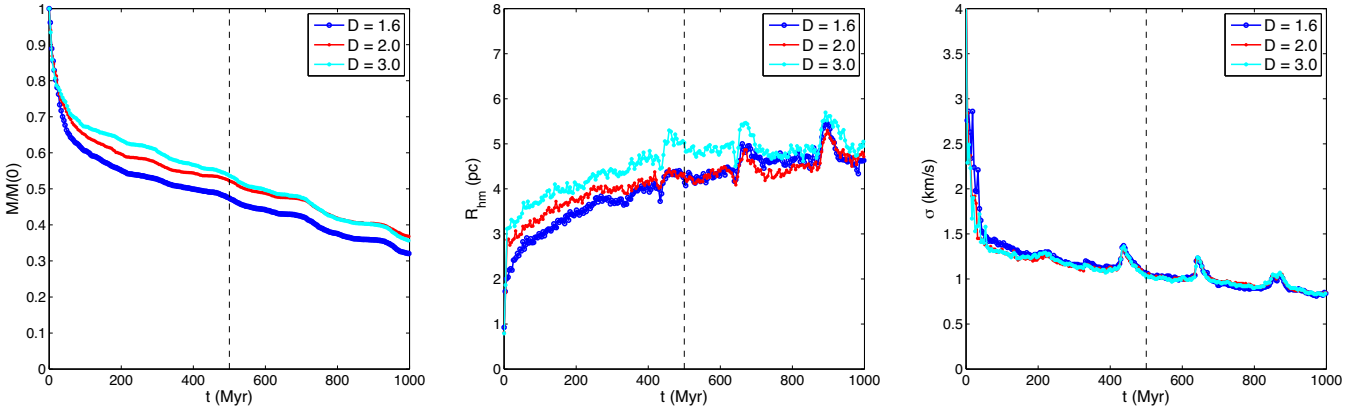

Figure 5. Evolution of the mass (left-hand panel), half-mass radius (middle panel) and velocity dispersion (right-hand panel) of initially supervirial clusters ($\alpha_{\rm vir} = 0.8$) on the outer orbit with different initial fractal dimensions. The dark blue, red and light blue lines show the results of the simulations of clusters with initial fractal degree $D = 1.6$, 2.0 and 3.0, respectively. The vertical black dashed line indicates the time $t_{\rm check}$ at which the properties have been evaluated in Fig. 4.

initial subcluster mass and size is 1/10th of the mass and size of the whole cluster, respectively, its relaxation time is about one order of magnitude smaller than the relaxation time of the entire system. It is then possible that, since the escape of stars from the subclusters is favoured, the overall relaxation time of the system in the early stages of evolution decreases, explaining the observed decreasing trend of retained mass for decreasing fractal degrees.

Similarly, the half-mass radius of the evolved clusters does not show a strong dependence on the initial fractal degree, with only a few per cent variation for different initial fractal dimension. On average, we found that the clusters are characterized by a bigger half-mass radius for increasing initial fractal dimension (middle panels of Fig. 4 and of Fig. 5), mirroring the trend observed in the retained mass fraction.

Of all the parameters considered in our analysis, the velocity dispersion of the cluster members is the one that resulted in being the least sensitive to the initial degree of clumpiness of the clusters. This result is shown in the right-hand panels of Figs 4 and 5. The trends of the velocity dispersion of the selected clusters essentially overlap and respond in the same way to the injection of kinetic energy owing to tidal shocks (see also the bottom right-hand panel of Fig. 2).

Finally, we note that these trends are similarly reproduced for clusters following both the inner and outer orbits.

3.2 Impact of the initial virial ratio on the long-term evolution

For the next step in our analysis, we grouped the simulated clusters accordingly to their initial virial ratio and looked for the presence of any obvious dependence of the evolved properties of the clusters on the initial value of $\alpha_{\rm vir}$. The results are shown in Fig. 6.

We found that the initially virialized clusters experience a smaller mass-loss rate than both supervirial and subvirial clusters of the order of 10 per cent (see left-hand panel of Fig. 6). This result is evident also in the left-hand panel of Fig. 7, in which we show the mass evolution of three realizations of clusters on the outer orbit as a function of their initial virial state for the first 1 Gyr of evolution. Once again, such a trend mirrors the value of the relaxation time at $t_{\rm check}$. We found that initially sub/supervirial clusters evolve with systematically smaller relaxation times from the very early stages. A collapsing system will then exhibit a shorter crossing time, inducing faster relaxation of the system. On the other hand, in a tidally limited system such as a star cluster in a galaxy it is possible that if the cluster is initially expanding the number of escapers in the early stages can

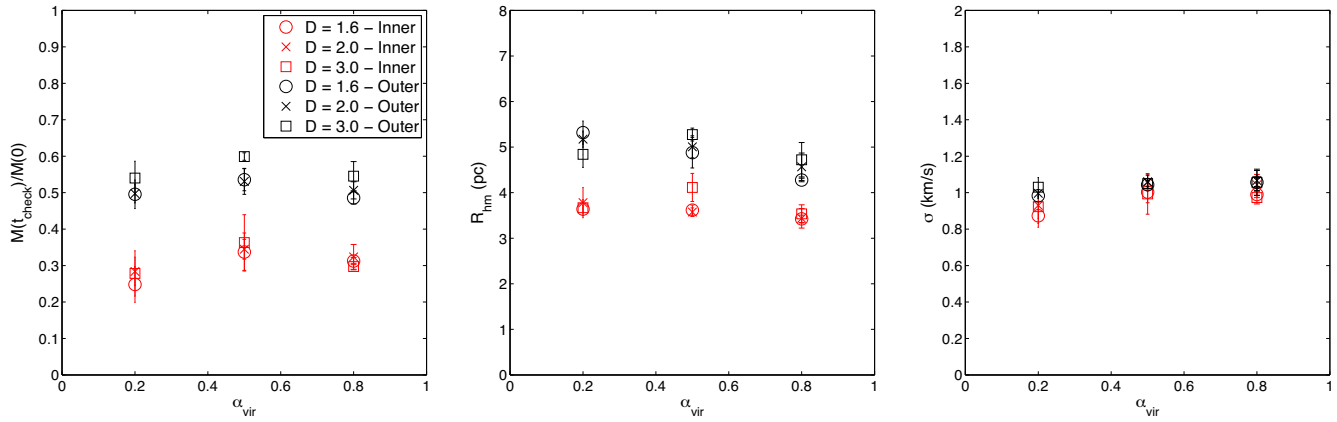

Figure 6. Left-hand panel: fraction of the initial mass retained by the star clusters at $t_{\rm check}$ as a function of the initial virial ratio $\alpha_{\rm vir}$ for clusters with different initial fractal degrees. The open circles, crosses and open squares show the average value for clusters with $D = 1.6$, 2.0 and 3.0, respectively. The red and black symbols show the results for the inner orbit and the outer orbit, respectively. Middle panel: half-mass radius at $t_{\rm check}$ as a function of the initial virial ratio $\alpha_{\rm vir}$ for clusters with different initial fractal degrees. Symbols and colours as in the left-hand panel. Right-hand panel: velocity dispersion of the cluster members at $t_{\rm check}$ as a function of the initial virial ratio $\alpha_{\rm vir}$ for clusters with different initial fractal degrees. Symbols and colours as in the left-hand panel.

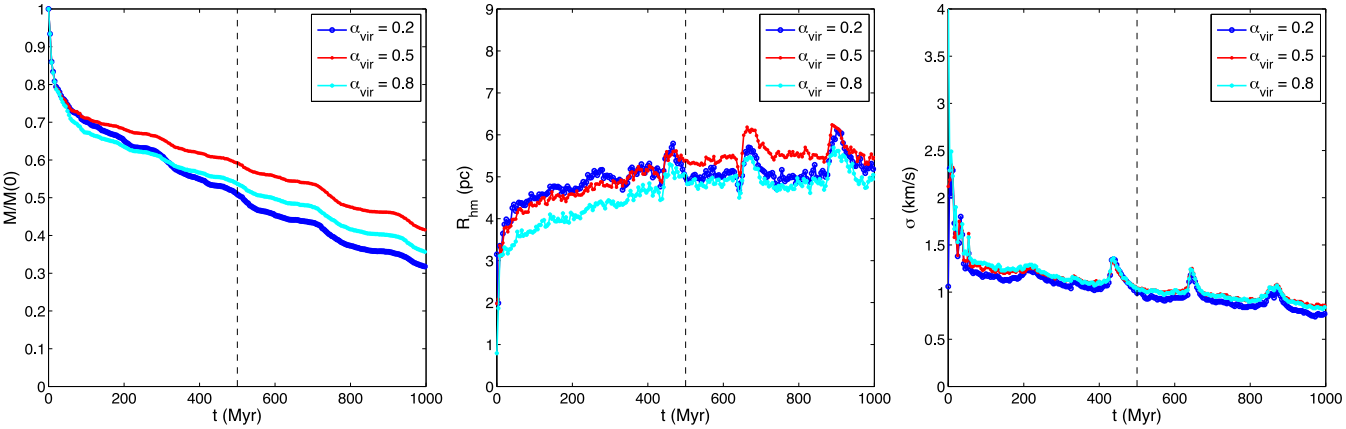

Figure 7. Evolution of the mass (left-hand panel), half-mass radius (middle panel) and velocity dispersion (right-hand panel) of initially spherical clusters ($D = 3.0$) on the outer orbit with different initial virial ratios. The dark blue, red and light blue lines show the results of the simulations of clusters with initial virial ratio $D = 0.2$, 0.5 and 0.8, respectively. The vertical black dashed line indicates the time $t_{\rm check}$ at which the properties have been evaluated in Fig. 6.

be enhanced, once again reducing the number of cluster members and hence the relaxation time of the system.

This trend is also reflected in the size of the clusters. Initially virialized clusters evolve with slightly bigger half-mass radii. However, we also note that such a variation is of the order of only a few per cent and is of the order of the variations associated with the random realizations of the clusters (see the middle panels of Figs 6 and 7).

Similar to the effect of the initial fractal dimension, the initial virial state of the clusters also does not significantly affect the evolution of the velocity dispersion of the cluster members.

Finally, we note that also in this case, the discussed trends are quite well reproduced for both the inner and outer orbits.

3.3 Impact of the initial degree of mass segregation on the long-term evolution

The results presented above are valid only for star clusters in which the initial masses are initially homogeneously distributed throughout the clusters, i.e. the mass of the stars do not depend on their distance from the cluster's centre. For the sake of completeness, we also evaluated the case of initially mass-segregated clusters. We considered the case of initially spherical virialized star clusters ($D = 3.0$, $\alpha_{\rm vir} = 0.5$) with different degrees of mass segregation S, namely $S = 0.0$, 0.5 and 1.0. These correspond to the cases of non-segregated, moderately segregated and fully segregated clusters, respectively. For this particular test, it is important to consider that setting the same value of the half-mass radius for all the different values of S would imply a much more disperse configuration for the clusters with $S = 1.0$. In order to avoid such an inconvenience and obtain a more consistent comparison of the results, we set the half-number radius for all the clusters to 2 pc. This gives an initial $r_{\rm hm} \simeq 1$ pc for the $S = 1.0$ model compared to $r_{\rm hm} \simeq 2$ pc for the $S = 0.0$ unsegregated model. Fig. 8 shows the distribution of the average stellar masses as a function of the distance from the centre of the cluster r for the cases considered. The results of the N-body simulations are shown in Figs 9 and 10.

The initial degree of mass segregation overall does not seem to play a very important role in the subsequent mass evolution of the clusters. The left-hand panel of Fig. 9 shows that the retained mass of the clusters at $t_{\rm check}$ slightly increases for increasing degree of

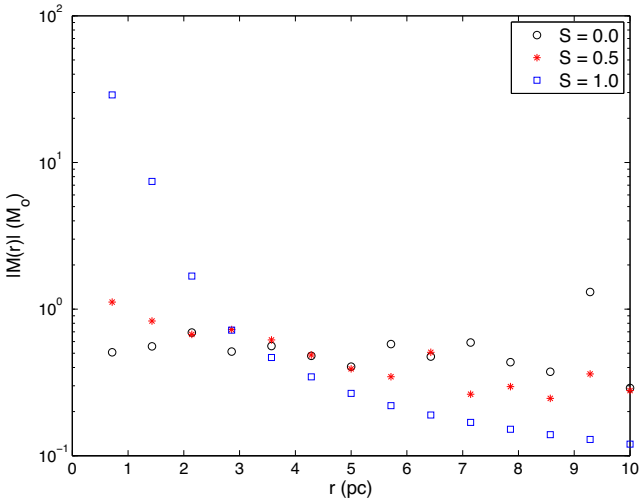

Figure 8. Distribution of the average stellar masses as a function of the distance from the cluster centre of mass for different degrees of mass segregation S. The open black circles, red stars and blue crosses show the average mass distribution for $S = 0.0$, 0.5 and 1.0, respectively.

primordial mass segregation. The time evolution of the clusters' mass on the outer orbit is reported in the left-hand panel of Fig. 10.

The half-mass radius decreases as the mass segregation increases (see Fig. 9). That is to be expected based on the way the clusters have been set up, where we have demanded the half-number radius to be the same for all the models. This means that the initial half-mass radius is smaller for greater degree of mass segregation. We see in Fig. 10 (middle panel) that, even though we see the usual early increase in half-mass radius as the clusters evolve, the half-mass radius for the segregated clusters remains smaller than for the unsegregated models for the whole evolution.

Regarding the velocity dispersion, we found slightly increasing values of the velocity dispersion at $t_{\rm check}$ for increasing degrees of primordial mass segregation (see right-hand panel of Fig. 9). Yet, the magnitude of such a variation is very small (right-hand panel of Fig. 10).

Such results can be interpreted by considering that, having fixed the half number radius to 2 pc, the primordial mass-segregated clusters are initially more compact than the non-mass segregated objects. As such, the segregated clusters grow to smaller half-mass radii, which in turn implies a smaller impact of the tidal field on the cluster evolution and an increased fraction of retained mass.

However, it is important to note that we would observe an opposite trend in retained mass fraction and half-mass radius as a function of primordial mass segregation if instead we fixed the initial half-mass radius to 2 pc, with fully segregated clusters being more easily destroyed by tidal interactions. In fact, in this case, segregated clusters start their evolution from more diffuse configurations, and hence, they are more easily stripped by tidal forces.

3.4 Impact of the tidal field on the long-term evolution

The results of the simulations suggest that the dependence of the different cluster properties on the initial conditions is quite similar for the inner and outer orbits, in the sense that the trends presented are observed in both cases. However, as mentioned above, the variations in the cluster properties linked to the different initial conditions are of the same order of magnitude as the intrinsic variations linked to the different realizations of the clusters, except for the case of primordial fully segregated clusters.

In all cases, the effect of varying D and $\alpha_{\rm vir}$ is outweighed by the impact of the tidal field on the long-term evolution of the clusters. All the cluster properties at $t_{\rm check}$ (mass, half-mass radius and velocity dispersion) show systematically smaller values for the inner orbit, which in turn reflects a more intense tidal field. Such a strong dependence is observed in particular for the mass and the half-mass radius of the clusters. In fact, the difference in the retained mass fraction at $t_{\rm check}$ for the clusters on the outer orbit can be up to about 40 per cent greater than for the clusters on the inner orbit, and this translates to smaller half-mass radii (typically of the order of 30 per cent smaller for the inner orbit). Of all the parameters considered in our analysis, the velocity dispersion of the cluster members is the property showing the smallest dependence on the initial conditions and the nature of the tidal field.

We note that the results presented are valid for clusters evolving along two different orbits within an LMC galaxy model, in which

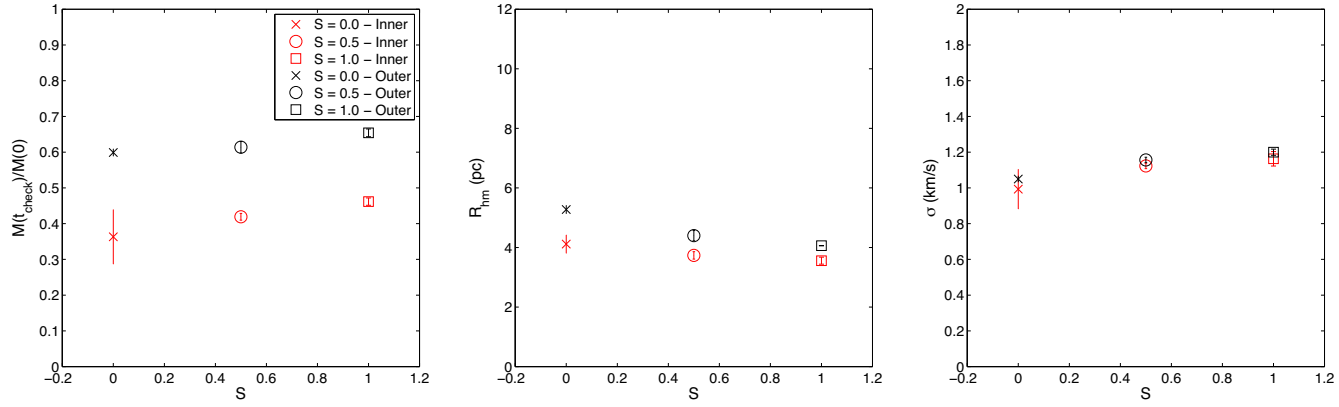

Figure 9. Left-hand panel: fraction of the initial mass retained by the star clusters at $t_{\rm check}$ as a function of the initial degree of mass segregation S for initially virialized spherical clusters. The open circles, crosses and open squares show the average value for clusters with $S = 0.0$, 0.5 and 1.0, respectively. The red and black symbols show the results for the inner and outer orbits, respectively. Middle panel: half-mass radius at $t_{\rm check}$ as a function of the initial degree of mass segregation S for initially virialized spherical clusters. Symbols and colours as in the left-hand panel. Right-hand panel: velocity dispersion of the cluster members at $t_{\rm check}$ as a function of the initial degree of mass segregation S for initially virialized spherical clusters. Symbols and colours as in the left-hand panel.

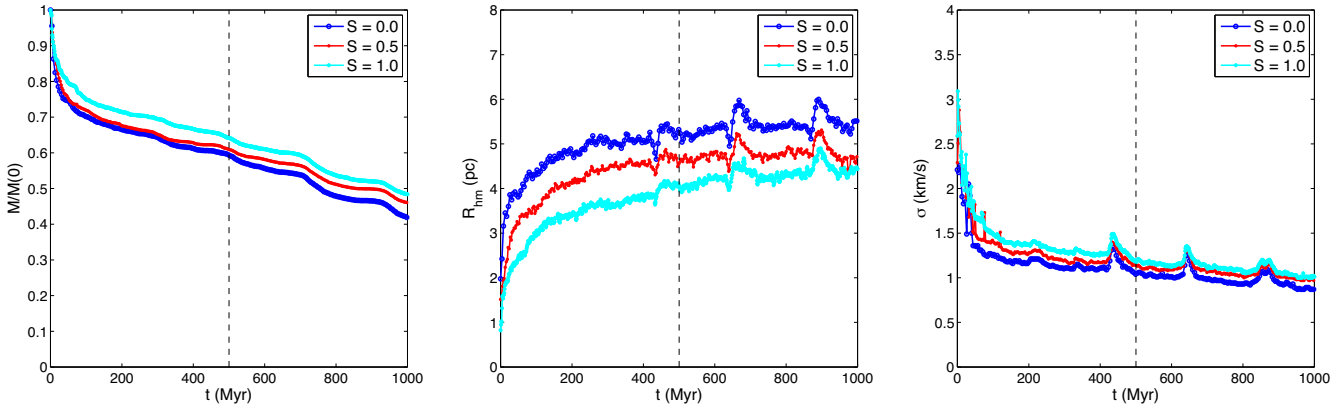

Figure 10. Evolution of the mass (left-hand panel), half-mass radius (middle panel) and velocity dispersion (right-hand panel) of initially spherical virialized clusters ($D = 3.0$, $\alpha_{\rm vir} = 0.5$) on the inner orbit with different initial degrees of mass segregation. The dark blue, red and light blue lines show the results of the simulations of clusters with initial $S = 0.0$, 0.5 and 1.0, respectively. The vertical black dashed line indicates the time $t_{\rm check}$ at which the properties have been evaluated in Fig. 9.

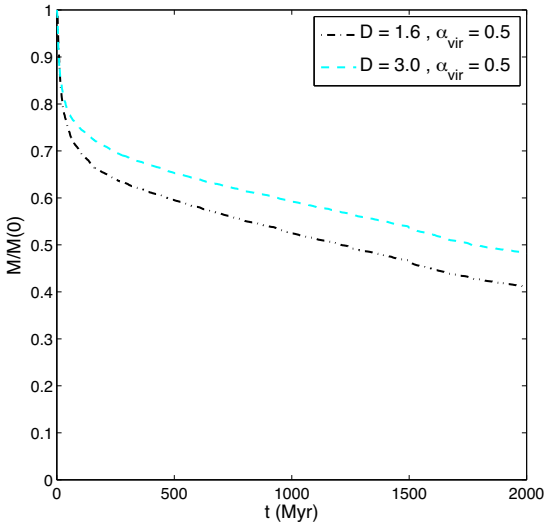

Figure 11. Evolution of the mass of clusters with initially $N = 100$ k stars and with different fractal dimension and virial ratio. The black dot–dashed line and the light blue dashed line show the result for clusters with ($D = 1.6$, $\alpha_{\rm vir} = 0.5$) and ($D = 3.0$, $\alpha_{\rm vir} = 0.5$), respectively.

the tidal forces are moderate. It is reasonable to expect that the impact of the tidal field would be even more important in the case of clusters subject to the more intense tidal field generated by a Milky Way model, with a dependence on the particular trajectory followed.

3.5 Results from bigger simulations

In order to identify any possible dependence of the results on the initial number of stars in the simulations, we evolved a set of larger clusters with $N = 100$ k. As a test, we ran two simulations of clusters following the inner trajectory with the following initial properties: one virialized clumpy cluster ($D = 1.6$, $\alpha_{\rm vir} = 0.5$) and one virialized spherical cluster ($D = 3.0$, $\alpha_{\rm vir} = 0.5$). For each of these cases, we neglected any primordial mass segregation ($S = 0.0$). The results of the N-body simulations are shown in Fig. 11 in terms of the evolution of the mass. After 2 Gyr of evolution, these more massive objects have still retained about half of their initial mass. At this time, the spherical virialized cluster has retained about 10 per cent more mass than the virialized clumpy cluster, a difference in good agreement with the results of smaller N-body simulations discussed above (see the left-hand panels of Figs 4 and 5). We found that the half-mass radius and velocity dispersion (not shown in the figure) show the same dependence on the initial conditions as found for the smaller simulations. These results suggest that the observed trends can be extended to more massive objects.

4 SUMMARY AND CONCLUSIONS

The main goal of this work is to quantify how different initial conditions affect the long-term evolution of star clusters in comparison with the effect of the galactic tidal field. In order to answer this question, we performed direct N-body simulations of star clusters characterized by different initial fractal degrees, virial ratios, degrees of mass segregation and following different orbits in the realistic gravitational field generated by an N-body galaxy. We chose two orbits with distinct properties and tidal histories in a galaxy model representative of the LMC, namely an inner orbit confined in the inner 2 kpc of the galaxy and an outer orbit extending up to about 6 kpc from the galactic centre. We generated clusters in initial clumpy configurations with different fractal dimensions D ($D = 1.6$, 2.0, 3.0) and with different initial virial ratios $\alpha_{\rm vir}$ ($\alpha_{\rm vir} = 0.2$, 0.5, 0.8). Furthermore, we modelled the effects of initial mass segregation S ($S = 0.0$, 0.5, 1.0). In order to quantify the effect of the stochastic realizations of the clusters with the different initial properties for each combination of initial conditions, we simulated three clusters generated by varying the random seed number for a total of 66 direct $N = 10$ k simulations of star clusters. On the top of these smaller simulations, we ran two additional $N = 100$ k simulations of clusters following the inner orbit with varying D and $\alpha_{\rm vir}$ and used the results to explore the dependence of the various properties of the star clusters on their initial mass.

We quantified the effect of the initial conditions on three important observable properties of star clusters, namely the mass, half-mass radius and velocity dispersion of the cluster members, extracting their value at a time $t_{\rm check}$ at which the clusters are in a 'mature' phase of evolution and yet still massive enough to avoid statistical small-number fluctuations. Our results for initially

unvirialized, clumpy and/or mass-segregated clusters can be summarized as follows:

(1) Initially spherical clusters experience a lower mass-loss rate if compared to initially very clumpy clusters, with average masses 10 per cent bigger in the spherical case at $t_{\rm check} = 500$ Myr. The half-mass radius does not show any clear dependence on the initial fractal degree, nor does the internal velocity dispersion.

(2) Initially virialized clusters have smaller mass-loss rates when compared to supervirial and subvirial clusters, with variations of the average values of retained mass of about 10 per cent at $t_{\rm check} = 500$ Myr. This translates into slightly larger half-mass radii for clusters in initial virial equilibrium, while the velocity dispersion does not show any obvious dependence on the initial virial state.

(3) Assuming the same distribution of the stellar number density, primordially mass-segregated clusters evolve with smaller half-mass radii and higher retained mass fractions if compared to unsegregated objects.

(4) As a general consideration, we found that the variation of the average values of the cluster parameters owing to the different initial conditions is of the same order of magnitude of the variation linked to the stochastic realization of the clusters of the same type.

(5) The effect of the galactic gravitational field has a major impact on the evolved cluster properties, with the clusters on the inner trajectory exhibiting systematically smaller values of mass, half-mass radii and velocity dispersion. For the specific case of the selected orbits, such variations are typically twice as big as the variations produced by the different initial conditions.

(6) The trends observed for the $N = 10$ k simulations are well reproduced also by larger $N = 100$ k simulations, suggesting that our results can be extended also to more massive clusters.

Such results indicate that for the study of the long-term evolution of star clusters in galaxies the initial conditions of the clusters have a secondary effect compared to the impact of their particular trajectory in the galaxy. Or, in other words, the tidal field dominates the long-term evolution and the common assumption of spherical, virialized clusters seems to be justified by the results of N-body simulations. However, the initial size of the clusters can influence the subsequent mass-loss rates and dissolution times (e.g. Gieles & Baumgardt 2008; Rossi et al. 2016). As noted by Renaud et al. (2017), for example, the tidal history of the clusters in the very early stages of evolution can be quite different compared to the present-day scenario. In fact, very old objects such as globular clusters initially evolved in forming galaxies, subject to tidal forces much smaller than those experienced by the clusters today. On the other hand, gas-rich environments could have enhanced tidal shock effects and increased destruction rates of star clusters (Gieles et al. 2006; Gieles & Renaud 2016). Furthermore, it is possible that the initial distribution of stars with the lowest fractal degree D considered in this study might not be as clumpy as the real situations within some giant molecular clouds. Also, in the early clumpy phases, the young clusters are embedded in the gas from which they formed and the removal of the gas itself due to stellar activity might have an important impact on the subsequent evolution.

Finally, considering that the extreme cases of primordial fully mass-segregated, supervirial clusters are unlikely, the results of this work suggest that some of the initial properties of star clusters such as virial state and clumpiness do not seem to play a major role in the long-term evolution of star clusters. However, other parameters such as the initial size and the details of the tidal histories in the early evolutionary stages of the clusters can greatly affect the present-day properties of star clusters in galaxies, justifying any attempt to obtain more realistic initial conditions for N-body simulations of star clusters in realistic tidal fields.

ACKNOWLEDGEMENTS

We thank the anonymousreferee for comments that we believe have contributed to an improved submission. This work was performed on the swinSTAR and gSTAR supercomputers at Swinburne University of Technology funded by Swinburne and the Australian Government's Education Investment Fund. LR acknowledges a CRS scholarship from Swinburne University of Technology.

REFERENCES

Aarseth S. J., 2003, Gravitational N-Body Simulations. Cambridge Univ. Press, Cambridge
Allison R. J., Goodwin S. P., Parker R. J., Portegies Zwart S. F., de Grijs R., 2010, MNRAS, 407, 1098
Bate M. R., Bonnell I. A., Bromm V., 2003, MNRAS, 339, 577
Baumgardt H., Makino J., 2003, MNRAS, 340, 227
Beasley M. A., Baugh C. M., Forbes D. A., Sharples R. M., Frenk C. S., 2002, MNRAS, 333, 383
Bekki K., Forbes D. A., Beasley M. A., Couch W. J., 2002, MNRAS, 335, 1176
Boley A. C., Lake G., Read J., Teyssier R., 2009, ApJ, 706, L192
Bonnell I. A., Davies M. B., 1998, MNRAS, 295, 691
Bonnell I. A., Bate M. R., Vine S. G., 2003, MNRAS, 343, 413
Bonnell I. A., Clark P., Bate M. R., 2008, MNRAS, 389, 1556
Bournaud F., Duc P.-A., Emsellem E., 2008, MNRAS, 389, L8
Caputo D. P., de Vries N., Portegies Zwart S., 2014, MNRAS, 445, 674
Dale J. E., Ercolano B., Bonnell I. A., 2012, MNRAS, 424, 377
Fujii M. S., 2015, PASJ, 67, 59
Gieles M., Baumgardt H., 2008, MNRAS, 389, L28
Gieles M., Renaud F., 2016, MNRAS, 463, L103
Gieles M., Portegies Zwart S. F., Baumgardt H., Athanassoula E., Lamers H. J. G. L. M., Sipior M., Leenaarts J., 2006, MNRAS, 371, 793
Girichidis P., Federrath C., Allison R., Banerjee R., Klessen R. S., 2012, MNRAS, 420, 3264
Goodwin S. P., Whitworth A. P., 2004, A&A, 413, 929
Gutermuth R. A., Megeath S. T., Myers P. C., Allen L. E., Pipher J. L., Fazio G. G., 2009, ApJS, 184, 18
Hurley J. R., Pols O. R., Tout C. A., 2000, MNRAS, 315, 543
Hurley J. R., Tout C. A., Pols O. R., 2002, MNRAS, 329, 897
Kravtsov A. V., Gnedin O. Y., 2005, ApJ, 623, 650
Kroupa P., 2001, MNRAS, 322, 231
Küpper A. H. W., Maschberger T., Kroupa P., Baumgardt H., 2011, MNRAS, 417, 2300
Lada C. J., Margulis M., Dearborn D., 1984, ApJ, 285, 141
Li Y., Mac Low M.-M., Klessen R. S., 2004, ApJ, 614, L29
Li H., Gnedin O. Y., Gnedin N. Y., Meng X., Semenov V. A., Kravtsov A. V., 2017, ApJ, 834, 69
Moeckel N., Bonnell I. A., 2009, MNRAS, 396, 1864
Parker R. J., Wright N. J., Goodwin S. P., Meyer M. R., 2014, MNRAS, 438, 620
Plummer H. C., 1911, MNRAS, 71, 460
Portegies Zwart S. F., McMillan S. L. W., Gieles M., 2010, ARA&A, 48, 431
Rathborne J. M. et al., 2015, ApJ, 802, 125
Renaud F., Gieles M., 2013, MNRAS, 431, L83
Renaud F., Bournaud F., Duc P.-A., 2015, MNRAS, 446, 2038
Renaud F., Agertz O., Gieles M., 2017, MNRAS, 465, 3622
Rieder S., Ishiyama T., Langelaan P., Makino J., McMillan S. L. W., Portegies Zwart S., 2013, MNRAS, 436, 3695
Rossi L. J., Bekki K., Hurley J. R., 2016, MNRAS, 462, 2861
Schneider N. et al., 2012, A&A, 540, L11

This paper has been typeset from a TEX/LATEX file prepared by the author.